

Modeling of Energy Losses During Cornering for Electric City Buses

Camiel J.J. Beckers¹, Igo J.M. Besselink¹ and Henk Nijmeijer¹

Abstract—Accurate energy consumption prediction is essential for optimal operation of battery electric buses. Conventional prediction algorithms do not consider energy losses during turning of the vehicle, which is especially relevant for city buses driving curvy routes. This paper presents a model describing steady-state cornering of such buses and analyses the additional energy consumption. The model includes multiple nonlinear effects, such as large steer angles, double rear wheels, and lateral load transfer. The resulting four nonlinear equilibrium equations are solved iteratively to obtain steady-state solutions. These reveal that both *cornering resistance* at the front wheels and *tire scrub* of the double rear wheels cause energy losses, varying as function of vehicle velocity and corner radius. Combination of the results with a recorded city trip of a battery electric bus reveals that these effects combined may account for 2.3% of the driveline energy consumption.

Index Terms—EV energy prediction, heavy-duty vehicle, tire energy losses, cornering

I. INTRODUCTION

In the past decade, Battery Electric Buses (BEBs) have emerged as an alternative for diesel-powered public road transport. BEBs are more environmentally friendly, without local pollution, and have the potential for a low total cost of ownership, due to the low running expenses [1]. However, efficient usage of the vehicles is essential to counter the high initial purchase costs. This poses a challenge for timetable schedulers, who have to take into account the charging strategies and limited driving range of the vehicles. This driving range is often uncertain and is influenced by several environmental and vehicle parameters, resulting in conservative, sub-optimal time tables and use of redundant vehicles.

A solution to this challenge is offered by developing more accurate energy consumption prediction algorithms. These algorithms reduce the uncertainty regarding the remaining driving range and possibly enable energy efficient dynamic scheduling. While procedures for prediction of energy consumption are extensively described in the literature, for example [2], [3], [4], [5], [6], almost all algorithms - often implicitly - assume straight line driving of the vehicle. This assumption is not always valid, especially when electric city buses are considered. The city routes contain many corners, which cause additional energy losses in the tires.

There are some studies that do consider corners in the energy consumption prediction. One example is found in

the paper of L. L. Ojeda, A. Chasse, and R. Goussault [6], where the effects of road curvature are included in the velocity profile construction. Still, the applied vehicle energy consumption model assumes straight-line driving.

Early literature indicates that cornering energy losses can be significant for articulated trucks [7]. There are several studies that aim to estimate and minimize these losses using vehicle dynamic models. Kobayashi et al. [8] describe a linearized single track model to analyze the cornering resistance of a vehicle with rear in-wheel motors. Likewise, Bhat et al. [9] derived the cornering resistance from a linearized single track model, with the objective to minimize energy losses by actively optimizing camber settings and steer angles. Maclaurin [10] analyzed the steering characteristics of six-wheel military vehicle. In this study, a more complex double track cornering model was adopted to compare skid steer to Ackermann steer, also considering energy consumption. A nonlinear double track model was used by Rill [11] to devise a torque vectoring strategy for passenger cars that is optimal in an energy consumption sense. However, this model still assumes linear tire forces and no load transfer.

Even though these studies quantify the cornering losses for particular cases to some extent, the contribution of these losses to the overall energy consumption is rarely considered. Furthermore, the models used are either entirely or partially linearized and do not consider load transfer between the tires of the vehicle. The assumptions underlying these models are no longer valid in small-radius corners, where tire side-slip angles can become large and lateral load transfer is significant. Furthermore, little of the literature on cornering losses is focussed specifically on buses.

In this paper, the energy losses that occur during cornering of a BEB are assessed by development of a nonlinear steady-state cornering model. Two physical effects that contribute to the energy consumption are considered: cornering resistance due to side-slip of the tires and vehicle, and tire scrub of the double rear tires. Real-world vehicle data is used to assess the relative impact of cornering energy losses on the total energy consumption of the vehicle driveline.

II. METHODOLOGY

Figure 1 shows a schematic top view of a BEB, with all relevant dimensions, individual tire velocities, and the resulting tire forces indicated. Additional to a standard double track model [12], the considered vehicle has double rear tires. The two sets of double rear tires each have angular velocities ω_L for tires 3 and 4, and ω_R for tires 5 and 6. In the depicted steady-state cornering situation, the vehicle velocity $v = |\vec{v}|$ is constant, as well as the cornering radius R . The front

¹Department of Mechanical Engineering, Eindhoven University of Technology, P.O. Box 513, 5600 MB Eindhoven, The Netherlands
c.j.j.beckers@tue.nl, i.j.m.besselink@tue.nl, h.nijmeijer@tue.nl
This project has received funding from the European Union's Horizon 2020 research and innovation programme under grant agreement No. 713771.

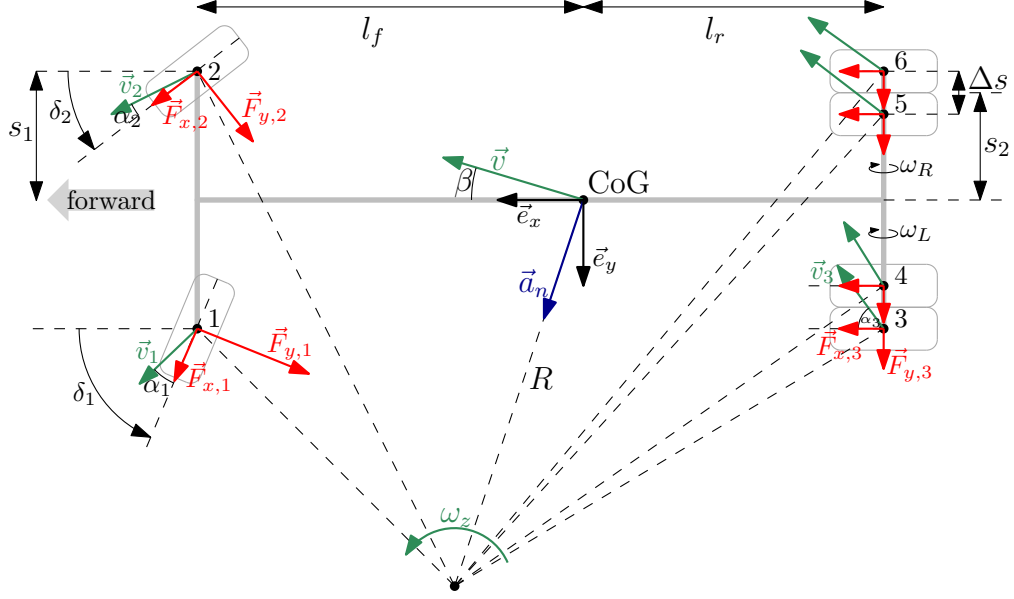


Fig. 1. Schematic top view of the vehicle. The vehicle chassis and tires are indicated with relevant dimensions l_f, l_r, s_1, s_2 , and Δs . For each of the six tires ($i = 1, \dots, 6$), the velocity vector \vec{v}_i , the longitudinal force $\vec{F}_{x,i}$, and the lateral force $\vec{F}_{y,i}$ are indicated, together with the respective side-slip angle α_i . A vehicle fixed axis system (\vec{e}_x, \vec{e}_y) has its origin in the CoG. The normal acceleration vector is indicated with \vec{a}_n .

wheels have a constant steer angle δ_1 and δ_2 , respectively, which is averaged as $\delta = \frac{1}{2}(\delta_1 + \delta_2)$. This results in a constant yaw-rate ω_z , a constant vehicle side-slip angle β , and a constant lateral acceleration $a_n = |\vec{a}_n|$. The goal of the steady-state cornering model is to determine the individual tire forces in this situation.

A. Kinematics

Given the degrees of freedom of the model $\underline{s} = [\delta, \beta, \omega_L, \omega_R]^T$ and the corner parameters (v, R) , the velocity components of the Center of Gravity (CoG) are given by

$$v_x = v \cos(\beta) \quad v_y = -v \sin(\beta) \quad \omega_z = \frac{v}{R} \quad (1)$$

with v_x the longitudinal vehicle velocity and v_y the lateral vehicle velocity. For further calculations, a multibody dynamics approach is applied. The velocity components are stored in a column \underline{v} such that

$$\vec{v} = \underline{v}^T \underline{\vec{e}} = [v_x \quad v_y \quad 0] \begin{bmatrix} \vec{e}_x \\ \vec{e}_y \\ \vec{e}_z \end{bmatrix}, \quad (2)$$

where \underline{v} indicates the column containing the coordinates that describe the velocity vector \vec{v} , and $\underline{\vec{e}}$ is the column of unit vectors that describe a vehicle-fixed axis system that has its origin in the CoG. Using the same notation, the position of each of the six tires with respect to the CoG is expressed as

$$\vec{p}_i = \underline{p}_i^T \underline{\vec{e}} \quad i = 1, 2, \dots, 6, \quad (3)$$

where the columns \underline{p}_i , containing the tire position coordinates, solely depend on the vehicle dimensions l_f and l_r which define the distance between the vehicle CoG and the front and rear axle respectively, and the track widths defined by s_1, s_2 , and Δs , which are indicated in Fig. 1.

The local tire velocity vector coordinates can be expressed in each of the tire-fixed axis systems according to

$$\underline{v}_i = \underline{A}(\delta_i) \left(\underline{v} + \begin{bmatrix} 0 \\ 0 \\ \omega_z \end{bmatrix} \times \underline{p}_i \right) \quad i = 1, 2, \dots, 6, \quad (4)$$

where $\underline{A}(\delta_i)$ denotes the direction cosine matrix that rotates the velocity vector from the vehicle-fixed frame to the tire-fixed frame as function of the steer angle δ_i and is defined by

$$\underline{A}(\delta_i) = \begin{bmatrix} \cos(\delta_i) & \sin(\delta_i) & 0 \\ -\sin(\delta_i) & \cos(\delta_i) & 0 \\ 0 & 0 & 1 \end{bmatrix}. \quad (5)$$

The front wheel steer angles δ_1 and δ_2 are assumed to be related through the Ackermann steering relation [13, p. 33], which allows for the kinematic relations

$$\delta_1 = \tan^{-1} \left(l \left(\frac{l}{\tan \delta} - s_1 \right)^{-1} \right) \quad (6)$$

$$\delta_2 = \tan^{-1} \left(l \left(\frac{l}{\tan \delta} + s_1 \right)^{-1} \right) \quad (7)$$

with $l = l_f + l_r$ the wheelbase of the vehicle. The steer angles of the rear wheels are zero, resulting in $\underline{A}(\delta_3) = \underline{A}(\delta_4) = \underline{A}(\delta_5) = \underline{A}(\delta_6) = \underline{I}$, where \underline{I} is the 3×3 unity matrix.

The column \underline{v}_i contains the coordinates of the local velocity vector with respect to the tire-fixed axis system, where the first and second component are denoted as $v_{x,i}$ and $v_{y,i}$, respectively. From these velocity components, the tire side-slip angle can be determined, according to

$$\alpha_i = \tan^{-1} \left(\frac{-v_{y,i}}{v_{x,i}} \right) \quad i = 1, 2, \dots, 6. \quad (8)$$

Furthermore, the longitudinal slip ratio is calculated as

$$\kappa_i = -\frac{v_{x,i} - r_{e,i}(F_{z,i})\omega_i}{|v_{x,i}|} \quad i = 1, 2, \dots, 6, \quad (9)$$

where the effective tire radius $r_{e,i}$ is considered to be a function of the vertical force $F_{z,i}$ acting on the tire. Longitudinal slip on the front wheels, which are not driven, is assumed to be zero. Therefore, $\kappa_1 = \kappa_2 = 0$.

B. Dynamics

In the calculation of the vertical tire forces, load transfer due to the longitudinal and lateral acceleration acting on the elevated CoG of the vehicle is taken into account. These accelerations are defined respectively as

$$a_x = \sin(\beta) \frac{v^2}{R} \quad a_y = \cos(\beta) \frac{v^2}{R}. \quad (10)$$

Subsequently, a pitch moment M_{pitch} and roll moment M_{roll} are defined that are perceived in the vehicle fixed axis system:

$$M_{pitch} = -h a_x m \quad M_{roll} = h a_y m, \quad (11)$$

where h is the height of the center of gravity with respect to the ground, and m is the total vehicle mass. A positive pitch moment M_{pitch} would shift part of the total vertical force from the rear axle to the front. This difference in vertical force is indicated by

$$\Delta F_{z,pitch} = \frac{M_{pitch}}{l_f + l_r}. \quad (12)$$

Likewise, a roll moment would result in a difference in the vertical force between the left and right track. The roll moment is distributed between the front and rear axle of the vehicle according to the roll moment distribution k_{dist} , resulting in separate expressions for the lateral load transfer at the front and rear axle:

$$\Delta F_{z,front} = k_{dist} \frac{M_{roll}}{2s_1} \quad (13)$$

$$\Delta F_{z,rear} = (k_{dist} - 1) \frac{M_{roll}}{2s_2}. \quad (14)$$

The total vertical force on each of the tires is a result of the static vertical force plus the effects of the two types of load transfer, resulting in

$$F_{z,i} = \frac{l_r}{2l} m g \pm \Delta F_{z,front} + \Delta F_{z,pitch}/2 \quad i = 1, 2 \quad (15)$$

$$F_{z,i} = \frac{l_f}{4l} m g \pm \frac{1}{2} \Delta F_{z,rear} - \Delta F_{z,pitch}/4 \quad i = 3, 4, 5, 6$$

with $l = l_f + l_r$ and g the gravitational acceleration.

A simplified version of Pacejka's Magic Formula [12, p. 7] is used to express both the longitudinal tire force $F_{x,i}$ and the lateral tire force $F_{y,i}$ of each tire as function of the slip conditions and the vertical force $F_{z,i}$, according to

$$F_{x,i} = f_{MF,x}(\kappa_i, F_{z,i}) \quad i = 1, 2, \dots, 6 \quad (16)$$

$$F_{y,i} = f_{MF,y}(\alpha_i, F_{z,i}) \quad i = 1, 2, \dots, 6. \quad (17)$$

Note that in this formulation $f_{MF,x}$ and $f_{MF,y}$ are considered to be independent. Thus, combined slip conditions are not taken into account. Furthermore, the longitudinal force expressions in $f_{MF,x}$ are slightly altered with respect

to the original Magic Formula to ensure monotonicity with respect to the slip ratio. This aids the convergence of Newton scheme, which will be described in Section II-C. Analysis shows that the alterations only effect extreme slip situations that do not occur in the final solutions of the model.

To describe the equilibrium equations governing the vehicle, the tire forces are transformed back to the vehicle axis system $\underline{\vec{e}}$ and are summed:

$$\begin{bmatrix} \sum F_x \\ \sum F_y \\ \sum F_z \end{bmatrix} = \sum_{i=1}^6 \underline{\vec{F}}_i = \sum_{i=1}^6 \underline{A}^{-1}(\delta_i) \begin{bmatrix} F_{x,i} \\ F_{y,i} \\ F_{z,i} \end{bmatrix}. \quad (18)$$

Four equilibrium equations are applicable. The first being the moment equilibrium around the vertical axis:

$$\sum M_z = \sum_{i=1}^6 p_i \times \underline{\vec{F}}_i = 0. \quad (19)$$

Secondly, the steady-state force equilibrium should hold for both the longitudinal and lateral direction:

$$\sum F_y - m a_y = 0 \quad (20)$$

$$\sum F_x - m a_x = 0. \quad (21)$$

The last equilibrium equation results from the assumption that a mechanical differential distributes the torque produced by the driveline evenly and lossless between a torque on the left rear axle T_L and a torque on the right rear axle T_R :

$$T_L = (F_{x,3}r_{e,3} + F_{x,4}r_{e,4}) \quad T_R = (F_{x,5}r_{e,5} + F_{x,6}r_{e,6})$$

$$T_L - T_R = 0. \quad (22)$$

C. Newton Iterations

To find the steady-state solution of the model, (19), (20), (21), and (22) are solved simultaneously for the degrees of freedom $\underline{s} = [\delta, \beta, \omega_L, \omega_R]^T$. The solution is found iteratively, using adapted Newton iterations [14] to minimize the error in each of the four equilibrium equations. Specifically,

$$\underline{s}_{k+1} = \underline{s}_k + \gamma (-\underline{J}(\underline{s}_k)^{-1} \underline{\varepsilon}(\underline{s}_k)) \quad k = 0, 1, 2, \dots \quad (23)$$

is evaluated repeatedly. In this equation, $\underline{\varepsilon}_k$ is the column containing the errors in the four equilibrium equations in respectively [N] and [Nm] as function of the current degrees of freedom \underline{s}_k . \underline{J} is the Jacobian matrix of $\underline{\varepsilon}_k$ with respect to the degrees of freedom \underline{s}_k , which is determined numerically using a finite difference method. The factor γ determines the adapted Newton step size and is in this case chosen inversely proportional to $|\underline{\varepsilon}_k|^2$.

As starting point for the iterative scheme, the solution of the linearized single track model at low velocity is used:

$$\underline{s}_0 = \begin{bmatrix} \tan^{-1}(l/\sqrt{R^2 - l_r}) \\ \tan^{-1}(-l_r/\sqrt{R^2 - l_r}) \\ v/r_e \\ v/r_e \end{bmatrix}. \quad (24)$$

When, after repeated evaluation of (23), the errors of the four equilibrium equations reach a certain tolerance the solution \underline{s}_k is considered to describe a steady-state situation.

III. MODEL RESULTS

The methods described in the previous section allow for the calculation of the individual tire forces of all six tires for any realistic cornering situation defined by the vehicle velocity v and the cornering radius R . A cornering situation of

TABLE I
VEHICLE PARAMETERS OF A TYPICAL BEB.

Parameter	Symbol	Value
Vehicle mass	m	15000 kg
Wheelbase	l	6 m
Longitudinal CoG position	l_f	3.5 m
CoG height above road	h	1.5 m
Average trackwidth	$2s_1 = 2s_2 + \Delta s$	2 m
Roll moment distribution	k_{dist}	1/4

$v = 20$ km/h and $R = 10$ m is considered for a typical BEB, of which the parameters are shown in Table I. Compared to conventional buses, BEBs are significantly heavier and have a higher CoG. By applying the methods in Section II-C to this situation, errors in the equilibrium equations of the model are minimized as displayed in Fig. 2. Furthermore, the starting solution of the linearized model and the final solution of the nonlinear model are summarized in Table II.

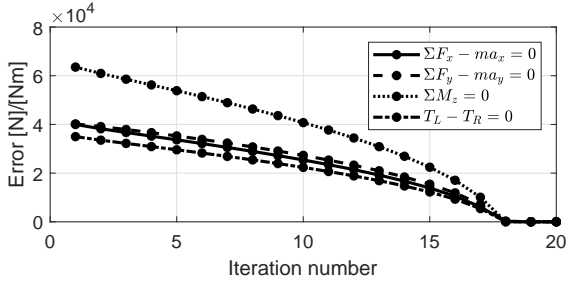


Fig. 2. Error in each of the four equilibrium equations as function of iteration number in the adapted Newton scheme.

TABLE II

COMPARISON OF THE EQUILIBRIUM SOLUTION OF THE LINEARIZED SINGLE TRACK MODEL AND THE NONLINEAR DOUBLE TRACK MODEL.

Model	δ [deg]	β [deg]	ω_L [RPM]	ω_R [RPM]
Lin. single track	31.0	-13.1	96.8	96.8
NL double track	31.8	-9.7	88.2	111.6
Difference	0.8	3.4	-8.6	14.8

The results show that the initial degree of freedom values, obtained from the linear single track model, serve as a suitable initial guess for the Newton scheme, but differ from the final results of the nonlinear model. The solution converges in 20 iterations and takes roughly 0.07 s to compute.

The model results for this small radius cornering situation, displayed in Fig. 3, show that the resulting vehicle side-slip angle and front wheel steering angles are significant. Consequently, the lateral tire force, indicated by red arrows originating from the center of these front wheels, is partially directed in the rearward direction. The tangential rearward components of these front wheel tire forces slow the vehicle down and are often referred to as *cornering resistance*.

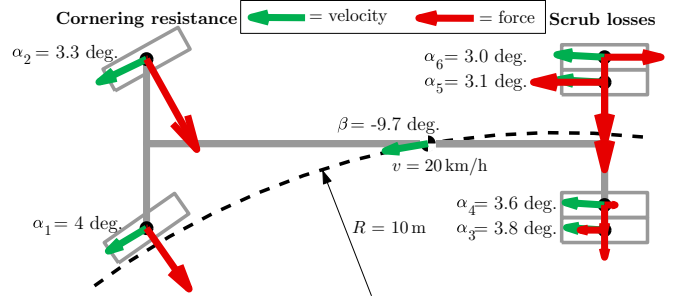


Fig. 3. Schematic top view of the vehicle and wheels (gray) with the solution of the steady-state cornering model for the parameters $v = 20$ km/h and $R = 10$ m. The dashed line indicates the path of the CoG of the BEB.

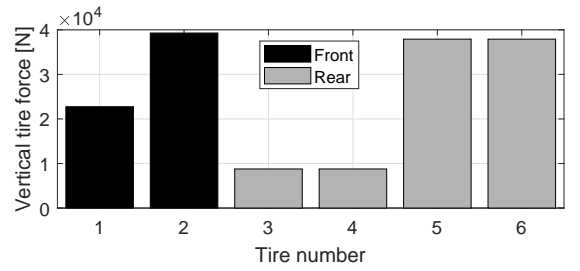


Fig. 4. Vertical tire force of the steady-state solution for each of the six tires in case $v = 20$ km/h and $R = 10$ m.

A second effect that is visible in Fig. 3 is *tire scrub*, due to the double rear wheels at each rear axle having a slightly different radius with respect to the corner center. This effect is visible as the opposing direction of the longitudinal tire forces on each of the sets of rear wheels. The inner wheel of each set creates a forward force, while the outer wheel creates a smaller rearward force. Together, the forces are positive and oppose the front wheel cornering resistance.

The figure also indicates the side-slip angles of the tires, highlighting the difference between the left and right side of the vehicle. Furthermore, the effects of lateral load transfer are evident in the vertical tire forces, displayed in Fig. 4.

A. Varying Cornering Situations

Due to both cornering resistance and tire scrub, extra power is required to corner a BEB, additional to the existing roadloads, such as rolling resistance and aerodynamic drag. Using the described model, this additional power due to both tire effects can be calculated for a range of cornering situations (v, R). The results for the cornering resistance power P_{cRes} , in Fig. 5a, show that this power is highest for high velocity, low radius cornering situations, and lower for either low velocity or large radius corners. The cornering resistance power can reach values of up to 20 kW. The power lost due to tire scrub P_{scrub} , displayed in Fig. 5b, is generally lower than P_{cRes} and shows less velocity dependence. Nevertheless, for $R < 20$ m values in excess of 0.4 kW are visible.

The powerlosses due to cornering resistance and tire scrub are summed and displayed in Fig. 6 as the combined cornering loss P_{loss} . The results are comparable to the results of solely the cornering resistance power (Fig. 5a), but with slightly higher values in the low velocity, small radius region. At large radii (straight line driving) the total cornering losses

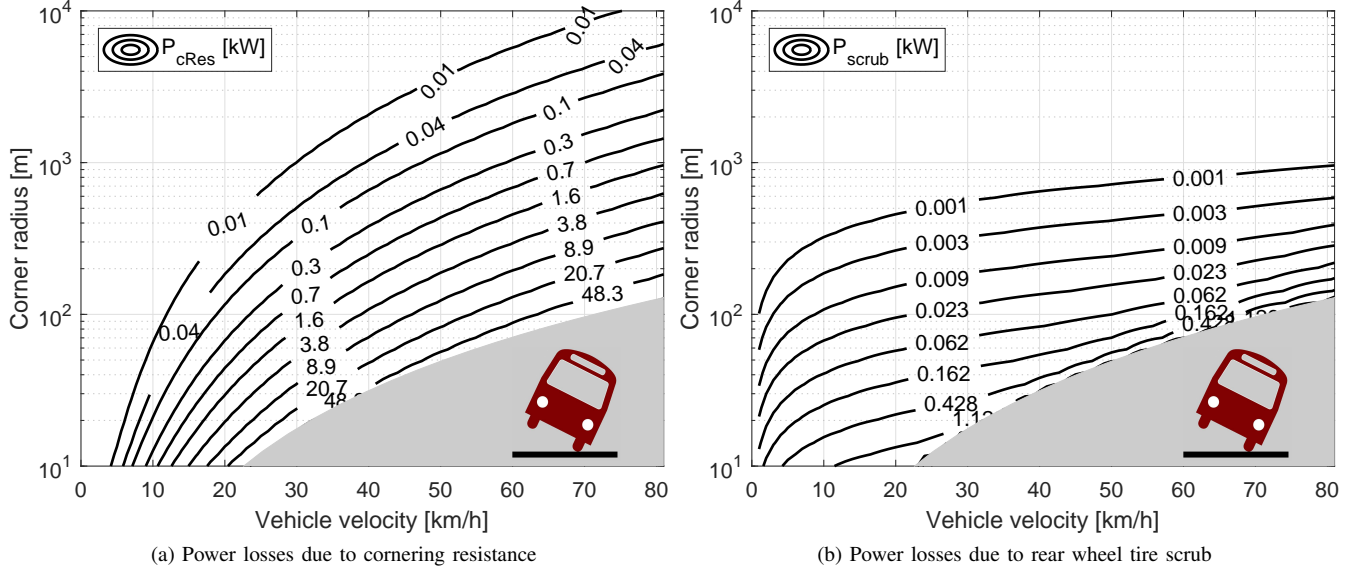


Fig. 5. Resulting energy losses due to cornering resistance (5a) and rear wheel tire scrub (5b) for a range of vehicle velocities and corner radii. Solutions for lateral accelerations of $a_y > 0.4g$ are not considered as the vehicle is close to roll over in this region.

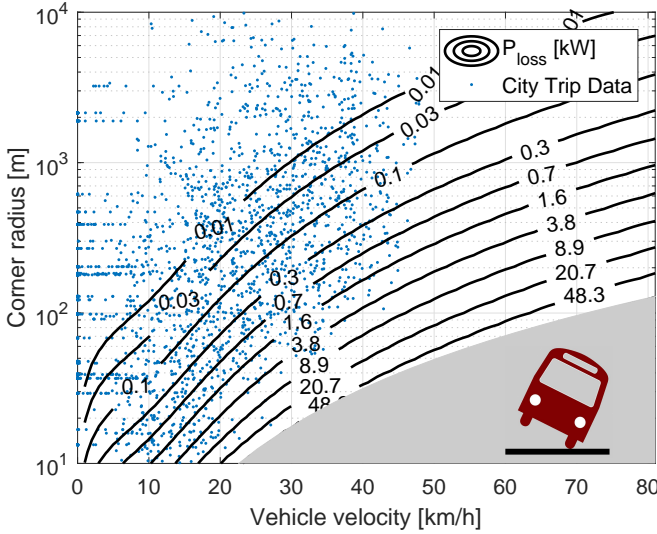


Fig. 6. Combined cornering losses as calculated by the model for various cornering situations. Recorded data from a city trip with a BEB indicates the occurrence of these situations. Solutions for lateral accelerations of $a_y > 0.4g$ are not considered due to vehicle roll.

are negligible, while at the minimal cornering radius of the vehicle (10 m), values in excess of 20 kW are reached.

Figure 6 also includes measured vehicle data to indicate whether the occurrence of these high-power cornering situations is realistic. The data was obtained from a monitored BEB, driving a city route. During the 60 minute trip, the vehicle velocity and GPS-position were recorded with a sampling rate of 1 Hz. In absence of both acceleration and yaw-rate sensors, the cornering radius is derived from the curvature of the recorded GPS-route. To this end, the raw GPS data is pre-processed by removing data-points with little intermediate distance and by applying a Savitzky-Golay low-pass filter [15] in the distance domain. Thereafter, the corner radius is calculated as the radius of the circle circumscribing

TABLE III
MEASURED DRIVELINE ENERGY $E_{driveline}$, CORNERING RESISTANCE ENERGY E_{cRes} , AND TIRE SCRUB ENERGY E_{Scrub} .

Energy	[kWh]	$1/E_{driveline}$
$E_{driveline}$	8.59	
E_{cRes}	0.171	1.99%
E_{Scrub}	0.029	0.34% +
$E_{cRes} + E_{Scrub}$	0.200	2.33%

the triangle spanned by a GPS measurement and its two neighbouring GPS points. The vehicle data in Fig. 6 shows that various combinations of corner radii and velocities up till 50 km/h occur.

During the recorded trip, the total driveline energy consumption was also measured. The combined cornering losses calculated for the measurement points shown in Fig. 6, can be summed over the length of the trip. This approach allows for a comparison between the total driveline energy consumption and the energy presumably dissipated by cornering losses, as displayed in Table III. The comparison reveals that during this particular city trip, approximately 2.3% of the driveline energy is dissipated by the cornering effects described here.

IV. DISCUSSION

The final results indicate that the cornering effects described by the model account for a significant 2.3% of the total driveline energy during the trip. It is also shown that the cornering losses can momentarily reach values of several kW during tight, fast corners. This is in accordance with the findings of Maclaurin [10], who simulated a vehicle of comparable weight and dimensions, and with the research performed by Gyenes, Williams, and Simmons [7], who simulated and measured the cornering losses of articulated trucks. The latter study concludes that for long freight trucks,

a maximum of 3% of the total energy consumption can be ascribed to cornering losses.

While the results appear plausible, some uncertainty in recorded cornering radius is expected, as the calculation relies on noisy GPS-data only. Nevertheless, the resulting corner situation distribution is assumed to be realistic.

The model results show that the cornering resistance losses are relatively large compared to the tire scrub losses. This indicates that even in heavy-duty vehicles that are not equipped with double rear tires, cornering losses might play an important role. It is therefore also surprising that these effects are hardly ever included in most energy consumption prediction algorithms for single-tire vehicles.

The equilibrium equations of the proposed model are solved using an iterative numerical method, where the solution of a simplified, linearized model is used as an initial guess. Even though this linearized model provides a decent starting point for the iterative scheme, the final solution of the nonlinear model differs from the solution of the linearized model. This indicates the importance of using a nonlinear model, without small angle assumptions, to simulate these tight cornering situations. Furthermore, the importance of using a double track model is highlighted by the simulation results in Fig. 3 and Fig. 4, where the difference in side-slip angles of the individual wheels and the difference in tire forces of the left and right track are evident.

Even though the presented model contains many nonlinearities, not all physical effects are taken into account. The tire model does not include turn slip or camber dynamics. Although these effects could be included in the Magic Formula [12, p. 183], they are assumed to have a negligible effect on the power losses. Additionally, turn slip is small when R is large compared to the tire width. Furthermore, the current model presented here does not include aerodynamic resistance or rolling resistance. Instead of quantifying the total resistance force, the model exclusively determines the tire losses additional to these conventional road-loads. Therefore, the model also does not account for the energy losses due to the deceleration and subsequent acceleration of the vehicle before and after the turn. Lastly, it is assumed that the losses during a dynamic corner situation can be represented by a summation of different steady-state cornering results.

While the main results indicate that the cornering losses are significant in one particular city trip with a BEB in city driving, more data from a variety of trips will have to be evaluated to obtain more conclusive results regarding the route-dependency of the results. Furthermore, dedicated steady-state cornering tests with a full size vehicle are considered as future work to match the outcome of the model with a measured energy consumption during cornering.

V. CONCLUSIONS

In this paper, the energy losses that occur during cornering of a BEB are modeled. The equations for a nonlinear steady-state cornering model for a BEB are derived and a solution method is proposed. The results indicate that during cornering of a BEB, both *cornering resistance* and

tire scrub contribute to additional power losses, where the former effect is more profound for most cornering situations. Combining the cornering model analysis outcome with the measured driveline energy consumption of a BEB reveals that the mentioned effects constitute a significant 2.3% of the total energy. Therefore, these effects should be taken into account to improve energy consumption prediction accuracy for BEBs.

REFERENCES

- [1] M. Pihlatie, S. Kukkonen, T. Halmeaho, V. Karvonen, and N.-O. Nylund, "Fully electric city buses - the viable option," in *IEEE Int. Elec. Veh. Conf. (IEVC)*. Florence, Italy: IEEE, Dec. 2014, pp. 1–8. [Online]. Available: <https://doi.org/10.1109/IEVC.2014.7056145>
- [2] J. Wang, I. J. M. Besselink, and H. Nijmeijer, "Battery electric vehicle energy consumption modelling for range estimation," *Int. J. Electr. Hybrid Veh.*, vol. 9, no. 2, pp. 79–102, 2017. [Online]. Available: <https://doi.org/10.1504/IJEHV.2017.085336>
- [3] C. De Cauwer, J. Van Mierlo, and T. Coosemans, "Energy consumption prediction for electric vehicles based on real-world data," *Energies*, vol. 8, no. 8, pp. 8573–8593, Aug. 2015. [Online]. Available: <https://doi.org/10.3390/en8088573>
- [4] R. Shankar and J. Marco, "Method for estimating the energy consumption of electric vehicles and plug-in hybrid electric vehicles under real-world driving conditions," *IET Intell. Transp. Syst.*, vol. 7, no. 1, pp. 138–150, Mar. 2013. [Online]. Available: <https://doi.org/10.1049/iet-its.2012.0114>
- [5] J. Vepsäläinen, K. Kivekäs, K. Otto, A. Lajunen, and K. Tammi, "Development and validation of energy demand uncertainty model for electric city buses," *Transp. Res. Part D Transp. Environ.*, vol. 63, pp. 347–361, Aug. 2018. [Online]. Available: <https://doi.org/10.1016/j.trd.2018.06.004>
- [6] L. L. Ojeda, A. Chasse, and R. Goussault, "Fuel consumption prediction for heavy-duty vehicles using digital maps," in *IEEE 20th Int. Conf. Intell. Transp. Syst.* Yokohama, Kanagawa, Japan: IEEE, Oct. 2017. [Online]. Available: <https://doi.org/10.1109/ITSC.2017.8317613>
- [7] L. Gyenes, T. Williams, and I. C. P. Simmons, "Power requirements of articulated vehicles under cornering conditions," Department of the Environment Department of Transport, Crowthorne, TRRL Supplementary Report 484, 1979. [Online]. Available: <https://trl.co.uk/sites/default/files/SR484.pdf>
- [8] T. Kobayashi, E. Katsuyama, H. Sugiura, E. Ono, and M. Yamamoto, "Direct yaw moment control and power consumption of in-wheel motor vehicle in steady-state turning," *Veh. Syst. Dyn.*, vol. 55, no. 1, pp. 104–120, Jan. 2017. [Online]. Available: <https://doi.org/10.1080/00423114.2016.1246737>
- [9] S. Bhat, M. M. Davari, and M. Nybacka, "Study on energy loss due to cornering resistance in over-actuated vehicles using optimal control," *SAE Int. J. Veh. Dyn. Stability, NVH*, vol. 1, no. 2, pp. 263–270, Mar. 2017. [Online]. Available: <https://doi.org/10.4271/2017-01-1568>
- [10] B. Maclaurin, "Comparing the steering performances of skid- and ackermann-steered vehicles," *Proc. Inst. Mech. Eng. Part D J. Automob. Eng.*, vol. 222, no. 5, pp. 739–756, May 2008. [Online]. Available: <https://doi.org/10.1243/09544070JAUTO567>
- [11] G. Rill, "Reducing the cornering resistance by torque vectoring," *Procedia Eng.*, vol. 199, pp. 3284–3289, 2017. [Online]. Available: <http://dx.doi.org/10.1016/j.proeng.2017.09.393>
- [12] H. B. Pacejka, *Tire and Vehicle Dynamics*, 3rd ed. Oxford: Butterworth-Heinemann, Apr. 2012. [Online]. Available: <https://www.sciencedirect.com/science/book/9780080970165>
- [13] I. Kageyama, "Steering system," in *Road Off-Road Veh. Syst. Dyn. Handb.*, 1st ed., G. Mastinu and M. Ploechl, Eds. Boca Raton: CRC Press, 2014, ch. 25, pp. 919–942. [Online]. Available: <https://www.taylorfrancis.com/books/9781420004908>
- [14] P. Y. Papalambros and D. J. Wilde, *Principles of Optimal Design*, 2nd ed. Cambridge: Cambridge University Press, 2000. [Online]. Available: <http://ebooks.cambridge.org/ref/id/CBO9780511626418>
- [15] A. Savitzky and M. J. E. Golay, "Smoothing and differentiation of data by simplified least squares procedures," *Anal. Chem.*, vol. 36, no. 8, pp. 1627–1639, Jul. 1964. [Online]. Available: <https://doi.org/10.1021/ac60214a047>